# L. Basic Studies of Ultrasonic Welding for Advanced Transportation Systems

*Principal Investigator: Zhili Feng*
*Oak Ridge National Laboratory*
*1 Bethel Valley Road, Oak Ridge, TN 37831*
*(865) 576-3797; fax: (865) 574-4928; e-mail: fengz@ornl.gov*

*Chief Scientist: James J. Eberhardt*
*(202) 586-9837; fax: (202) 587-2476; e-mail: James.Eberhardt@ee.doe.gov*
*Field Technical Manager: Philip S. Sklad*
*(865) 574-5069; fax:(865) 576-4963; e-mail:skladps@ornl.gov*

*Participants:*
*H. Wang, X. Zhang M. L. Santella, and E. A. Kenik, Oak Ridge National Laboratory*
*W. Zhang, Oakland University*

---

*Contractor:* Oak Ridge National Laboratory
*Contract No.:* DE-AC05-00OR22725

---

## Objective

- Develop a fundamental understanding of the ultrasonic welding (UW) process.
- Establish process conditions to optimize joint properties of aluminum alloys for auto body applications.
- Explore opportunities for joining dissimilar materials.
- Explore the feasibility of ultrasonic processing in other novel and unique situations in materials processing, such as metal powder consolidation, producing functionally graded components, and modifying surface properties.

## Approach

- Perform UW experiments to develop correlations of process parameters with joint properties.
- Characterize details of joint microstructures.
- Model the fundamental interactions of ultrasonic waves with solids.

## Accomplishments

- Determined the acoustic energy distribution by means of infrared thermography.
- Investigated the geometric effects on ultrasonic energy generation and dissipation during the welding process.
- Initiated experimental study on residual stress distribution in the bonding region.
- Developed an efficient computational model to study the acoustic energy distribution in the welded workpiece.

## Future Direction

- Continue welding process development for dissimilar materials, including joining of amorphous metals.
- Study the structure-property relationship of joints.

- Model the acoustic energy distribution in the weld joint.
- Study the residual stress distribution in the bonding region.
- Assess the ability of ultrasonic processing for low-temperature metal powder compaction and consolidation.

## Introduction

Ultrasonic welding (UW) uses high frequency mechanical vibrations to produce a solid-state metallurgical bond (weld) between metals. The basic process setup is illustrated in **Figure 1** for typical spot weld configuration. An electro-mechanical converter converts high-frequency electric current to mechanical vibration. The mechanical vibration is then modulated and amplified by the booster/horn before it is applied to the overlapping workpiece through the vibration of the sonotrode. A moderate clamping force is applied to ensure the mechanical vibration is transferred to the sheet-to-sheet interface (the faying surface) where the weld is created. Typically, the mechanical vibration is at 20–40 kHz with an amplitude range of 5–50 μm. The power delivered to the workpiece is in the range of several hundred to several thousand watts.

**Figure 2** illustrates the essential underlying mechanisms involved in the formation of the metallurgical bond at the workpiece interface during

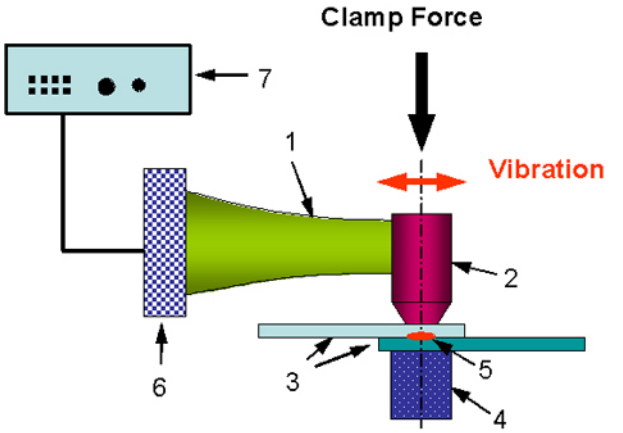


1 – Welding Horn 2 – Sonotrode
3 – Workpiece 4 – Anvil
5 – Weld 6 – Piezoelectric transducer
7 – High freq electric current generator

**Figure 1.** Schematic setup of ultrasonic welding process.

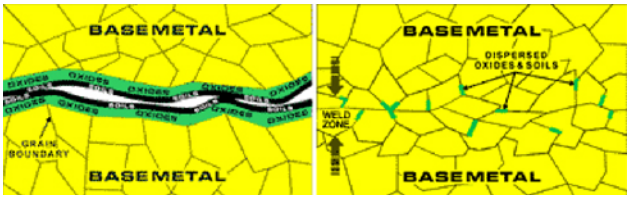


**Figure 2.** Schematic representation of bond interface before (left) and after (right) UW.

ultrasonic welding. The combination of normal clamp pressure and literal mechanical vibration results in several important effects at the workpiece interface. The lateral mechanical vibration introduces relative motion at the interface. The frictional action at the interface due to the relative motion and the normal pressure breaks the surface oxides and other contaminants. As result, clean metal surfaces are brought into contact under pressure. Frictional heating also occurs at the bond interface. The heating promotes both localized deformation and diffusion in the region where the pressure is applied. When the process conditions are right, metallurgical bond is formed without melting at the bonding interface. The self-cleaning nature of UW and its ability to form metallurgical bonds without melting are two important advantages of the process.

UW creates a joint without bulk melting. Thus, ultrasonic weld is inherently immune to welding defects associated with the solidification in various fusion welding processes (electric resistance spot welding, arc welding, laser welding etc). Solidification induced defects such as solidification cracking and porosity can be a major quality problem for a number of high-performance light-weight structural materials used in automotive body structures. In addition, UW is ideal for joining dissimilar metals such as Al to steel, Al to Mg, metal to metal composite that has been extremely difficult for the conventional fusion welding processes. Because melting is avoided, the ultrasonic welding process is much more energy efficient. UW has attracted considerable attention in the auto industry as an important enabling joining technology for

assembling structural components made of aluminum alloys, magnesium and other high-performance lightweight materials.

In our research performed in FY04, it was observed that the ultrasonic weld quality depends strongly on a number of geometric factors such as the weld location, the shape and size of the workpiece, and the sonotrode vibration direction relative to the workpiece. Under certain circumstances, cracking occurs at unexpected locations. Destruction of prior welds by subsequent welding was also observed. These observations suggested that the acoustic wave propagation and reflection in the workpiece being welded are very complicated and would result in considerable weld-to-weld quality variations.

In FY05, the program focused on investigating the acoustic energy distribution during welding. By utilizing the real-time infrared (IR) thermography technique, localized temperature rise in the workpiece during UW was observed and recorded as a function of time. The influence of the geometry factors on the energy distribution was experimentally investigated to elucidate possible causes for the observed weld quality variations. In addition, an efficient elasticity based computational modeling approach was developed to further the understanding of the acoustic energy distribution in the workpiece.

This report is divided into two parts. The first part deals with the experimental study of the acoustic energy distribution in the workpiece and its correlation to the weld quality. The second part of the report describes the theoretical treatment and computational modeling results of the acoustic energy distribution.

## Experimental Investigation of Acoustic Energy Distribution

### Welding

All welding trials were conducted on a Sonobond® ultrasonic welder. The machine operated at 20kHz and had a maximum rated power output of 2500W. Al6111 and Al5754, two aluminum alloys widely used in the automotive industry, were used for this investigation. Welds were made on 25-mm-wide and 100-mm-long coupons. This is a standard coupon dimension commonly used by the auto industry for weldability testing of spot welds. The nominal thickness of the workpiece was 1 mm. The weld was made in the overlap configuration, as shown in **Figure 3**. The overlap distance and the location of the weld were varied to investigate the geometry effects.

The basic ultrasonic bonding process parameters were: 2400W, 70psi, and 0.5 second.

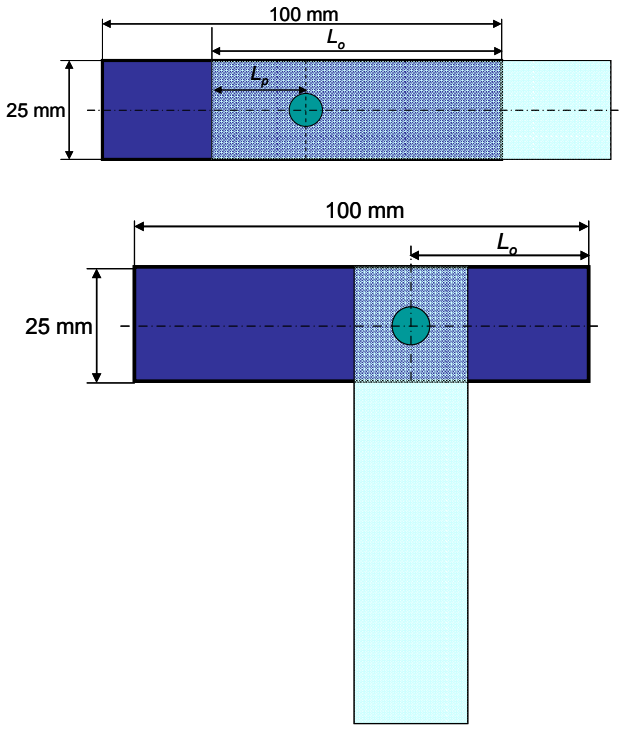


**Figure 3.** Weld coupon dimensions used in the study. Different overlap distance, *Lo*, and the weld position, *Lp*, were varied in the experiments.

### IR Thermography Measurement

A Raytheon, Radiance HS®, mid-IR (3-5 μm) camera was used to monitor the heat generation and diffusion in the weld samples. The temperature history of the weld sample was recorded at 60 frames per second, with a field of view of 256 x 256 pixels. During welding, the IR camera was aimed at the top surface of the specimen. In some tests, a water-soluble black paint was coated on the observing surface to reduce surface reflection and other interferences from the environment. Both the spatial distribution and the temporal variation of the temperature field were used to infer how the heat

(the dissipative part of the acoustic energy) is generated and distributed during UW.

## Results and Discussions

In last year's study, unforeseen cracking phenomenon was observed during ultrasonic welding of Al5754 alloy. The occurrence of such unusual cracking was highly repeatable in the welding trials. The location of the cracks, while generally away from the weld, is highly dependent on the geometric factors such as the overlapping distance and the position of the weld relative to the edge of the specimen. For example, as shown in **Figure 4**(a), when the overlap distance was at 75 mm and the weld position was at 35 mm, the cracking occurs at a distance approximately 20 mm away from the weld. On the other hand, when the overlap distance was at 35 mm and the weld position was at 20 mm, the cracks were lined up with the weld – **Figure 4**(b). In both cases, cracks form near the edge of the specimen, and they are not connected to the weld. Such a cracking pattern implies that the acoustic energy density in the weld sample does not monotonically decrease as the distance to the applied acoustic energy source (i.e., weld center) increases. Rather, sporadic high acoustic energy concentration spots exist in the welded workpiece.

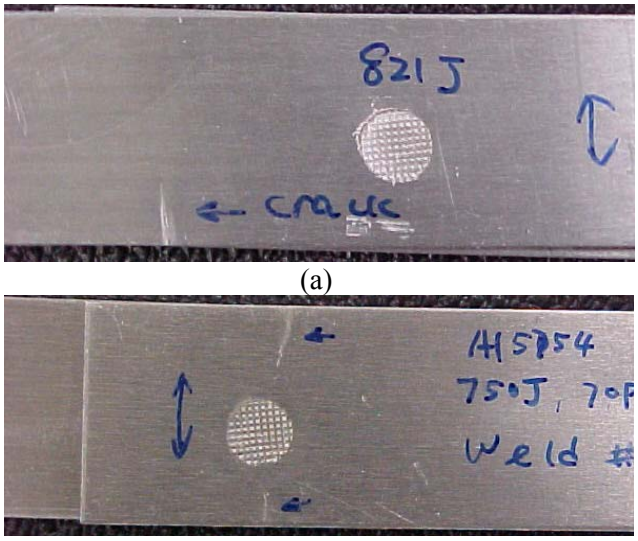


(a)

(b)

**Figure 4.** Unusual cracking during ultrasonic bonding of Al5754. The vibration direction of the sonotrode is along the width direction of the workpiece, as indicated by the vertical arrow marks.

Using the IR thermography, we were able to correlate the cracking phenomenon to localized temperature rise at the cracking location. **Figure 5** shows the temperature distribution in making the weld shown in **Figure 4**(a), as measured by IR thermography. There is clearly localized heating (the "hot spot") in the region where cracking occurred.

The same test was repeated with Al6111. While much less cracking was observed when welding Al6111, the localized heating behavior was consistent with Al5754 as shown in **Figure 6**.

Therefore, the localized heating is common to the Al alloys used in the experiment, although the cracking tendency is dependent upon the type of Al alloy.

It is well known that failure or cracking of materials results in heat generation as the stored elastic energy and plastic work is released and converted to thermal energy. The occurrence of the hot spot without cracking in Al6111 samples suggests that the localized heating away from the weld region is not caused by the cracking process. Rather, it indicates the existence of sporadic acoustic energy concentration points away from the weld region due to the complicated acoustic wave propagation and reflection behavior in the workpiece. The cracking (and the localized heating) is the result of the highly concentrated acoustic vibration.

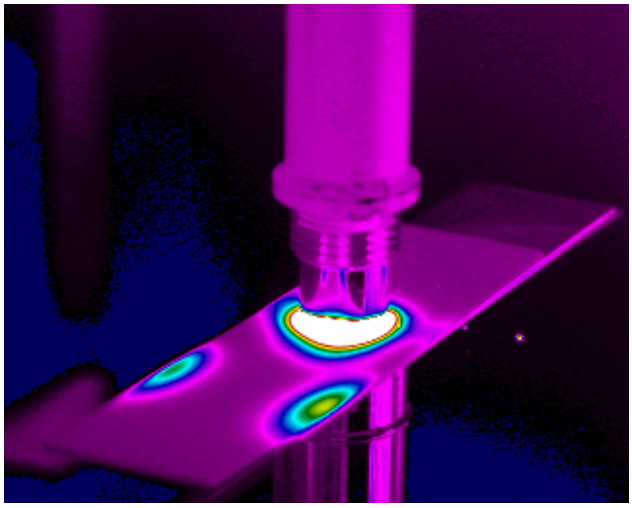

**Figure 5.** Pseudo color image of temperature distribution during ultrasonic welding of Al5754. Overlap distance: Lo=75 mm; weld position: Lp=35mm.

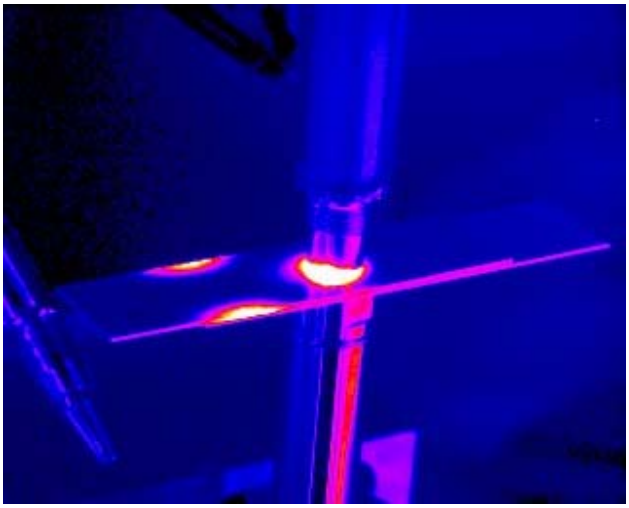

**Figure 6.** Pseudo color image of temperature distribution during ultrasonic welding of Al6111. Testing condition was identical to that in Figure 5.

To further elucidate the causes of the sporadic acoustic energy concentration spots, the following additional experiments were performed.

In the welding trials shown in **Figure 5**, the two Al sheets overlap each other and the hot spot is located within the overlapping region. Therefore, a potential cause for the localized heating would be the rubbing motion between the two Al workpieces in the hot spot area during ultrasonic welding. To test such hypothesis, welding trials were performed in which the bottom Al workpiece was rotated 90 degrees to form the T-stack up configuration. The result is shown in **Figure 7**. Clearly, the locations of hot spots are similar to the case in **Figure 5** and **Figure 6**. However, they are outside the overlapping region. This confirms that the localized heating and the subsequent cracking are not due to the mechanical interference between the two workpieces, but rather due to the acoustic vibration within the upper workpiece.

**Figure 8** shows a very different heating pattern when the stack-up order of the T-configuration was changed. In this case, the vertical piece of the T was on top of the horizontal piece. In other words, the vertical piece was in contact with the vibrating sonotrode, and the horizontal piece was in contact with the stationary anvil on the bottom. The unusual heating pattern was not observed.

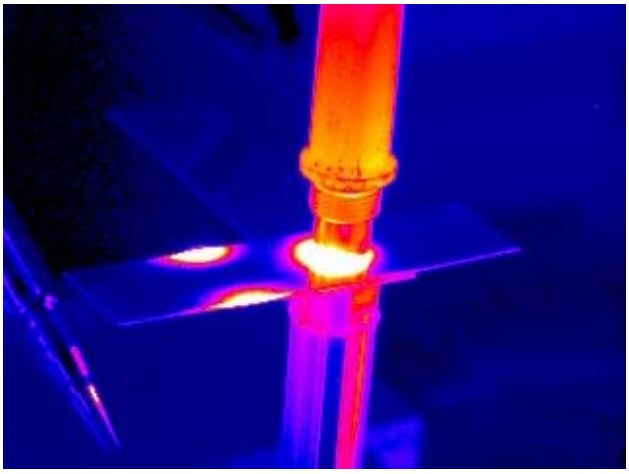

**Figure 7.** Pseudo color image of temperature distribution of T-stack up weld. Al 5754. The vertical piece sits on the bottom anvil. The horizontal piece is in contact with the upper sonotrode. The unusual localized heating occurs in the horizontal piece.

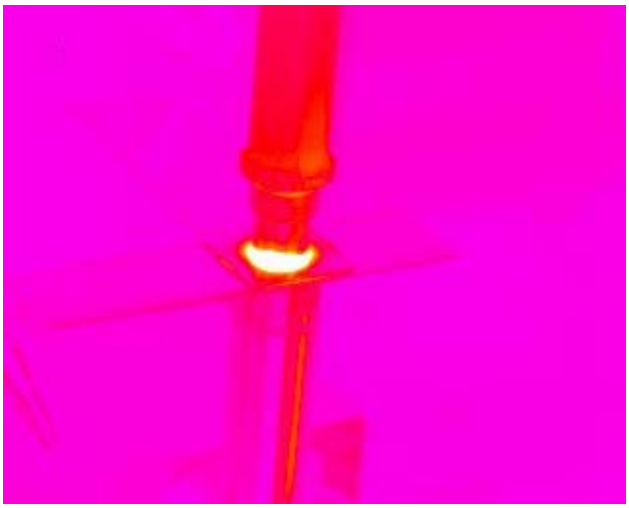

**Figure 8.** Pseudo color image of temperature distribution of T-stack up weld. Al 5754. The vertical piece is on the top. No unusual heating was observed.

In another test, the orientation of both workpieces was rotated 90 degrees such that the vibration direction of the sonotrode was in parallel to the length direction of the workpiece. The unusual heating was not observed, as shown in **Figure 9**.

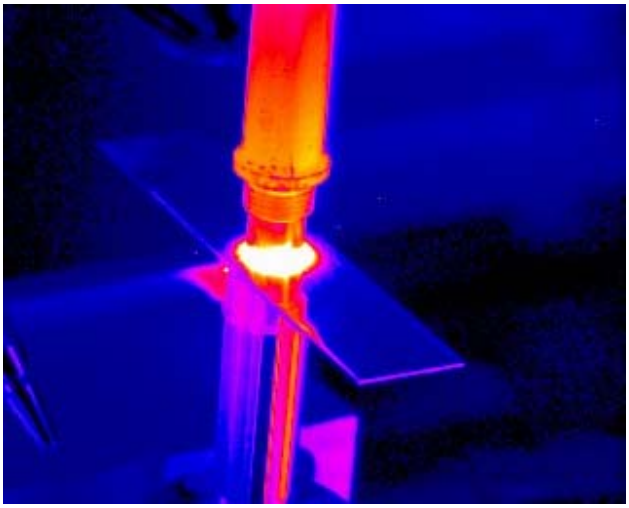

**Figure 9.** Pseudo color image of temperature distribution when both workpieces are lined to the vibration direction of the sonotrode. Al 5754.

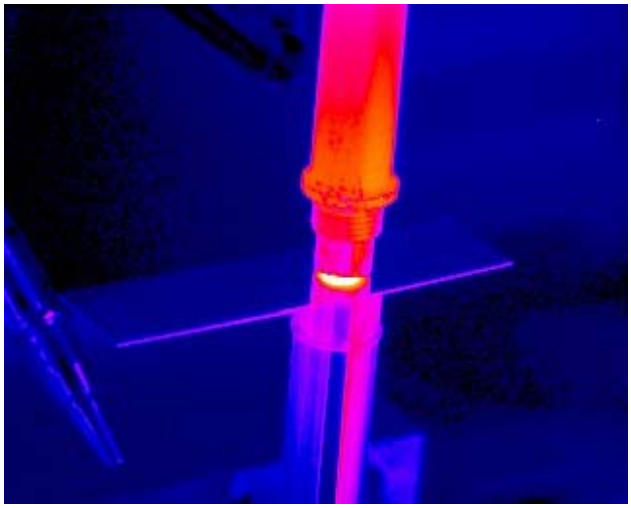

**Figure 10.** Pseudo color image of temperature distribution when only one Al sheet is used. Al 5754.

**Figure 10** shows the case when only one Al piece is used in the test. There was no unusual heating. This suggests that the concentration of the acoustic energy and thereby the observed unforeseen heating/cracking are related to the existence of unbounded interface between the two Al workpieces underneath the sonotrode. This is further supported by the fact that the unusual heating/cracking occurred in the early stage of the bonding process as illustrated in **Figure 11**, when the metallurgical bonding is not formed or relatively weak.

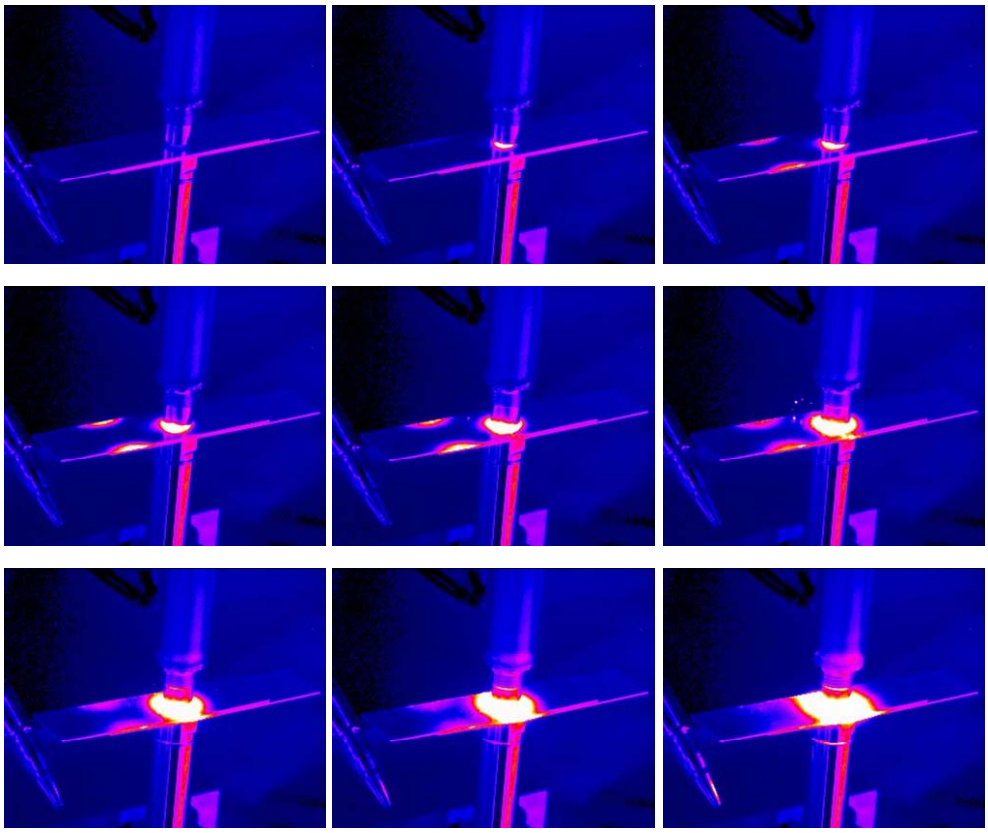

**Figure 11.** Sequential IR thermography image shots during ultrasonic welding.

## Modeling of Acoustic Energy Distribution

### Theoretical Treatment of Thin-Plate Vibration Pertaining to Ultrasonic Welding

Assume a thin plate situated in a three-dimensional rectangular coordinate system, (*x, y, z*), with thickness in the *z* direction. The plate is bounded by the planes $z = h$ and $z = -h$ and the thickness of the plate is $H = 2h$ at the start. Let *U, V, W* be the displacements of the plate in *x, y, z* directions respectively. We use the elastic model for high-frequency extensional vibrations of plate by Kane and Mindlin [J. Appl. Mech. 23 (1956) A-277-283]. In this model, it is proposed that the displacements in *x* and y directions are independent of the thickness of plate and the displacement in *z* direction varies linearly along *z* with no displacement at the middle plane of the plate. Hence, the three displacements can be written as

$$\begin{aligned} U(x,y,z,t) &= u(x,y,t) \\ V(x,y,z,t) &= v(x,y,t) \\ W(x,y,z,t) &= \frac{z}{h} w(x,y,t) \end{aligned} \tag{1}$$

where *u, v, w* is the so-called plate-displacements at the mid plane of the plate.

By introducing a constant multiplier to the thickness strain, Kane and Mindlin obtained the following plate-displacement system of equations of motion:

$$\begin{aligned} &(\lambda+2G)u_{xx} + Gu_{yy} + (\lambda+G)v_{xy} + \frac{\pi}{\sqrt{3}H}\lambda w_x + \frac{T_1}{H} = \rho u_{tt} \\ &Gv_{xx} + (\lambda+2G)v_{yy} + (\lambda+G)u_{xy} + \frac{\pi}{\sqrt{3}H}\lambda w_y + \frac{T_2}{H} = \rho v_{tt} \\ &G(w_{xx}+w_{yy}) - \frac{\sqrt{3}\pi}{H}\lambda(u_x+v_y) - \frac{\pi^2}{H^2}(\lambda+2G)w + \frac{3T_3}{H} = \rho w_{tt} \end{aligned} \tag{2}$$

where $\lambda$, $G$ are Lame's constants, $\rho$ is the mass density, $H = 2h$ is the thickness of the plate, $T_1, T_2, T_3$ are the components of surface traction in *x, y* and *z* directions.

Eq. (2) can be used to study the vibration of the workpiece under the acoustic excitation of a sonotrode during ultrasonic welding. Our model focuses on the distribution of the acoustic energy in the workpiece outside of the region underneath the sonotrode. Hence, the acoustic excitation from the sonotrode is assumed to be a temporal harmonic oscillation surface traction and its amplitude exhibiting exponential decay in the spatial domain from the center of the acoustic excitation. The temporal oscillation represents the vibration applied to a weldment throughout the process. The exponentially decaying spatial distribution of the amplitude represents that the vibration is concentrated in an area between the sonotrode and the anvil. The choice of a continuous surface traction is to avoid difficulties in solving Eq. (2) arising from spatial discontinuities.

In ultrasonic welding, strong friction exists at the interface of the two workpieces. This friction is simplified in the model by a damping term in each equation of motion in Eq. (2). Then the elastic model for ultrasonic welding is

$$\begin{aligned} &(\lambda+2G)u_{xx} + Gu_{yy} + (\lambda+G)v_{xy} + \frac{\pi}{\sqrt{3}H}\lambda w_x + C_1 e^{-\alpha\left[(x-x_s)^2+(y-y_s)^2\right]}\sin\omega t = \rho u_{tt} + \gamma u_t \\ &Gv_{xx} + (\lambda+2G)v_{yy} + (\lambda+G)u_{xy} + \frac{\pi}{\sqrt{3}H}\lambda w_y + C_2 e^{-\alpha\left[(x-x_s)^2+(y-y_s)^2\right]}\sin\omega t = \rho v_{tt} + \gamma v_t \\ &G(w_{xx}+w_{yy}) - \frac{\sqrt{3}\pi}{H}\lambda(u_x+v_y) - \frac{\pi^2}{H^2}(\lambda+2G)w + C_3 e^{-\alpha\left[(x-x_s)^2+(y-y_s)^2\right]}\sin\omega t = \rho w_{tt} + \gamma w_t \end{aligned} \tag{3}$$

where $\omega$ is the vibration angular frequency of the force applied to the weldment, $(x_s, y_s)$ is the center of the welding spot on the weldment, $C_1$, $C_2$, $C_3$, $\alpha$, $\gamma$ are nonnegative constants. It can be shown that the kinetic energy density of the plate on the *xy*-plane becomes

$$T(x,y,t) = \rho h\left(u_t^2 + v_t^2 + \frac{1}{3}w_t^2\right) \tag{4}$$

and the potential energy density of the plate on the *xy*-plane becomes

$$V(x,y,t) = h\left\{\lambda\left(u_x + v_y + \frac{\pi}{h\sqrt{12}}w\right)^2 + 2G\left(u_x^2 + v_y^2 + \frac{\pi^2}{12h^2}w^2\right) + G\left[\frac{1}{3}\left(w_x^2 + w_y^2\right) + \left(u_y + v_x\right)^2\right]\right\} \tag{5}$$

## Model Application to UW process

We now consider a rectangular plate. Let the spatial domain of the functions *u, v* and *w* be $[0, A]\times[0, B]$. In UW process, the sides of weldment are free. Hence, at the four sides of the rectangular plate we propose zero normal stresses and zero shear stresses along z-direction. The boundary conditions for Eq. (3) pertaining to the ultrasonic welding experiment of this study are:

$$\begin{aligned} &(\lambda + 2G)u_x + \lambda v_y + \frac{\pi\lambda}{h\sqrt{12}}w = 0 \\ &u_y - v_x = 0 \\ &w_x = 0 \end{aligned} \tag{6}$$

at the boundaries x = 0 and x = A,

and

$$\begin{aligned} &\lambda u_x + (\lambda + 2G)v_y + \frac{\pi\lambda}{h\sqrt{12}}w = 0 \\ &u_y - v_x = 0 \\ &w_y = 0 \end{aligned} \tag{7}$$

at the boundaries *y = 0* and *y = B*. The initial conditions for Eq. (3) in our UW model are

$$u(x,y,0) = v(x,y,0) = w(x,y,0) = u_t(x,y,0) = v_t(x,y,0) = w_t(x,y,0) = 0 \tag{8}$$

Eqs. (3), (6)-(8) forms a closed mathematical system of initial boundary problem of a system of linear partial differential equations.

For aluminum alloy, the following material constants are used in the model.

$$\begin{aligned} &\lambda = \frac{\sigma E}{(1+\sigma)(1-2\sigma)}\frac{N}{m^2}, \quad G = \frac{E}{2(1+\sigma)}\frac{N}{m^2}, \\ &E = 7.0404172\frac{N}{m^2}, \sigma = 0.34, \rho = 2700\frac{kg}{m^3}, \\ &H = 0.001m, A = 0.1m, B = 0.025m, \\ &x_s = 0.065m, y_s = 0.0125m \\ &\omega = 169646.01Hz \end{aligned}$$

The above system equations of elastic vibration and associated boundary conditions were solved numerically using the method of lines with central differences in the spatial discretization and variable-stepsize variable-order backward differentiation formulas in the time integration. Examples of the calculated vibration and energy distribution in the workpiece are presented below.

In the examples presented here, the dimensions of the rectangular plate and the location of the acoustic excitation are from the actual welding tests described in the experimental part of this report, to allow for comparison of the modeling results with the IR temperature measurement. Specifically, the plate dimensions were 25-mm wide, 100-mm long, and 1-mm thick. The position of the acoustic excitation, denoted Lp in **Figure 3**, was 35 mm. In the model and simulation coordinates the excitation is $x$ = 65 mm. Also, the damping coefficient representing the friction action of the sonotrode was assumed to be 20 times of the mass density of the material ($\gamma$=20$\rho$).

**Figure 12** shows the out-of-plane displacement of the plate (z-displacement) at six different moments during a cycle of elastic wave propagation, as calculated by the model. The direction of the driving excitation from the sonotrode is in the width direction of the plate (y-axis in the figure). This corresponds to the testing case shown in **Figure 5** and **Figure 6**. The calculated maximum vibration amplitude is concentrated at a particular location in the plate – near the edge of the plate and away from the excitation location. **Figure 13** shows the corresponding distribution of the sum of the kinetic and the potential energy density in the plate, averaged over the period of vibration. It is evident that the energy distribution in the plate is not uniform but rather sporadic. The predicted maximum energy locations are near the edge of the plate, which is consistent with the IR thermography experimental observations.

**Figure 14** and **Figure 15** show a different case where the driving vibration direction is in the length direction of the plate (x-axis); all other conditions are identical to the previous modeling case. This corresponds to the testing case showing in **Figure 9**. The time-averaged energy density in the plate is completely different from the previous modeling case. Not only the location of the maximum energy density is changed, the overall energy density in the plate is also considerably lower. Again, this is consistent with the experimental observations.

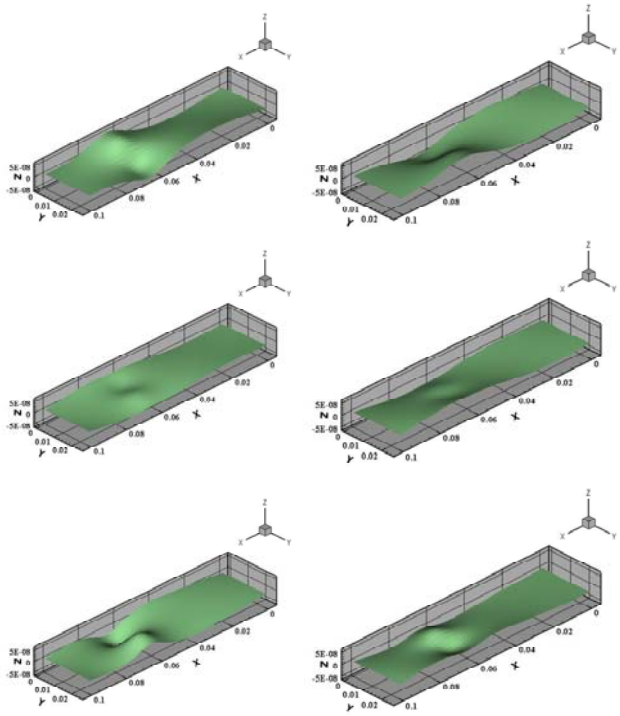

**Figure 12.** Vibration of the plate in the thickness direction (z-axis) during UW when the driving vibration is in the direction of y-axis. Acoustic excitation locates at x=0.065m and y=0.0125m.

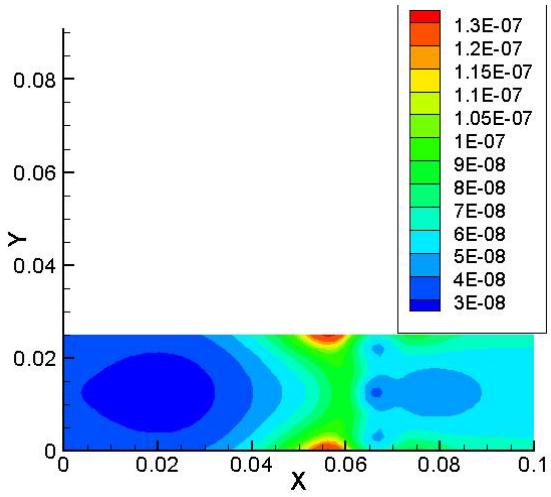


**Figure 13.** Distribution of the time-averaged sum of the kinetic and potential energy density in the plate during UW when the driving vibration is in the direction of y-axis.

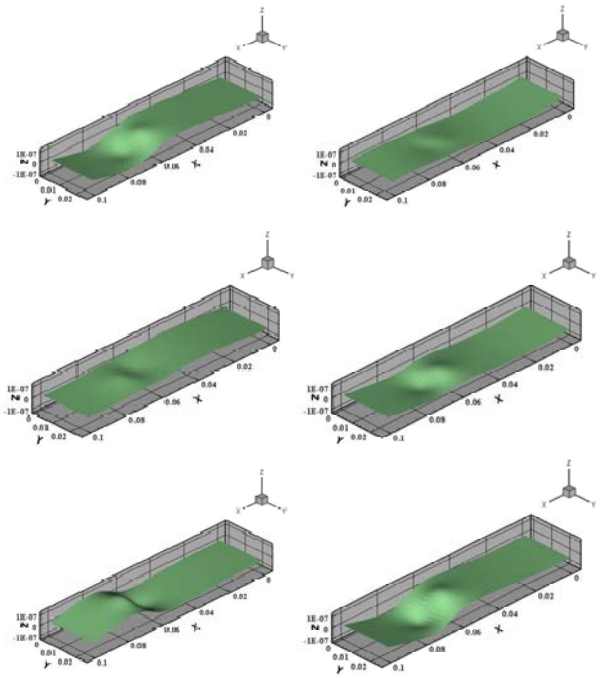

**Figure 14.** Vibration of the plate in the thickness direction (z-axis) during UW when the driving vibration is in the direction of x-axis. Acoustic excitation locates at x=0.065m and y=0.0125m.

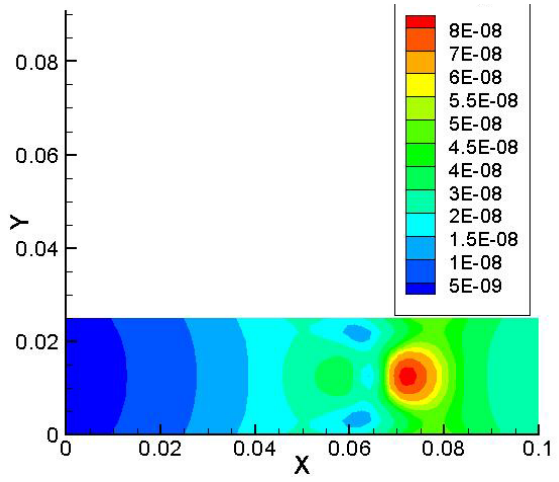


**Figure 15.** Distribution of the time-averaged sum of the kinetic and potential energy density in the plate during UW when the driving vibration is in the direction of x-axis.

Further studies are planned in FY06 to establish the validation of the model on a more rigorous base.

## Summary

In FY05, high-speed IR thermography and computational analysis based on the elastic high-frequency extensional vibration model made it possible to investigate the localized acoustic energy distribution and heat generation during the ultrasonic welding process. The causes for the formation of unforeseen hot spot and cracking have been identified, and factors contributing to the acoustic energy generation and dissipation in the welded samples have been determined.

The research in FY06 will continue on understanding of the fundamentals of the process, as well as the factors controlling them, for the eventual optimization and intelligent control of the UW process for application in the automotive industry. We will continue on the IR thermography study of the ultrasonic joining process, including the multi-weld interactions, the effects of the thickness and coupon geometry. We will also continue on developing the computational models for the UW process to interrogate the fundamental factors contributing to the formation of the metallurgical bonding. Finally, we will explore the use of ultrasonic energy for low-temperature metal compaction and consolidation.